Nuclear Materials and Energy 33 (2022) 101277

Contents lists available at ScienceDirect

Nuclear Materials and Energy

journal homepage: www.elsevier.com/locate/nme

Turbulence in the near scrape-off layer towards the L-mode density limit in ASDEX-Upgrade

G. Grenfell [a,*], P. Manz [a,b], G.D. Conway [a], T. Eich [a], J. Adamek [c], D. Brida [a], M. Komm [c], T. Nishizawa [a,d], M. Griener [a], B. Tal [a], U. Stroth [a,e], the ASDEX Upgrade team [a]

[a] Max–Planck-Institut fur Plasmaphysik, Boltzmannstr. 2, Garching, Germany
[b] Institute of Physics, University of Greifswald, Felix-Hausdorff-Str. 6, 17489 Greifswald, Germany
[c] Institute of Plasma Physics of the CAS, Za Slovankou 3, 182 00 Prague 8, Czech Republic
[d] Research Institute for Applied Mechanics, Kyushu University, Kasuga 816-8580, Japan
[e] Physik-Department E28, Technische Universität München, 85747 Garching, Germany

ARTICLE INFO

Keywords:
Turbulence
Scrape-off layer
Electrostatic probes
Tokamaks
Density limit
Detachment

ABSTRACT

The L-mode density limit in ASDEX Upgrade is investigated with focus on the scrape-off layer. We observe a chain of events that involves the collapse of the $E \times B$ outer shear layer (just outside the separatrix), widening of the electron pressure fall-off length, outer divertor detachment, density shoulder formation, reduction and flattening of the parallel Mach number, and enhanced turbulent cross-field transport. The latter effect was associated with higher amplitude density fluctuations at low frequencies, where the turbulent cross-phase between density and velocity fluctuations pointing radially outward was favourable.

1. Introduction

The density limit in tokamaks refers to the maximum achievable density before the plasma disrupts [1]. Such boundary imposes great restrictions for ITER and future reactors since the fusion reaction rate is proportional to the square of the plasma density, while disruptions will not be tolerable in these devices. Density limit is not exclusive to tokamaks, as it is also observed in stellarators [2,3] and reverse field pinches [4]. Generally, the limit is preceded by a chain of events that invariably lead to edge cooling and the rise of global MHD instabilities [5]. The onset of this process, however, is not well understood. Enhanced radial turbulent transport has been reported experimentally [6–8], presumably leading to the initial cooling necessary to trigger the final stage until the radiative collapse takes place.

In this view, turbulence plays a decisive role. An important question follows. Why does turbulent transport become more important near the limit? This question was addressed directly or indirectly in several publications, e.g., [9–12]. In general, different effects can explain this behaviour, although they do not necessarily exclude each other. First, near the limit, the plasma edge becomes more collisional, and that has an impact on turbulence [9]. Collisionality typically makes the response of the nearly unhindered motion of electrons along the field lines less efficient in damping pressure perturbation. In the outer midplane, where interchange effects can induce charge separation, the hampered electron response could lead to the growth of the interchange instability. The competition between these two effects is described by the turbulence parameter $\alpha_t \propto q^2 n_e / T_e^2$ [9,11], where q is the edge safety factor, n_e is the plasma density, and T_e the electron temperature. Large α_t would result in higher radial transport as turbulence becomes more interchange dominated [9]. In addition to the collisionality, electromagnetic effects could also play a role near the limit as the plasma beta increases. Turbulence simulations often show catastrophically large transport when resistive ballooning modes become electromagnetic [13]. In fact, the transition where turbulence at high collisionality also becomes electromagnetic has been proposed as the main mechanism leading to the critical edge cooling before the L-mode density limit [10], describing very well experimental observations [11]. Finally, the gradual weakening of turbulence stabilization by $E \times B$ shear flows as electron response becomes less adiabatic is also thought to be a key mechanism leading to high cross-transport prior to the limit [14]. The decreased adiabaticity impacts turbulent transport directly as well as indirectly by damping zonal flows [8,15], which otherwise would have a stabilizing effect on turbulence.

This paper focuses on profiles and turbulence evolution of the scrape-off layer (SOL), more precisely the near SOL, i.e., just outside the separatrix, for various densities towards the L-mode density limit. Steep gradients and long connection lengths characterize this region.

* Corresponding author.
E-mail address: gustavo.grenfell@ipp.mpg.de (G. Grenfell).

https://doi.org/10.1016/j.nme.2022.101277
Received 30 June 2022; Received in revised form 6 October 2022; Accepted 7 October 2022
Available online 18 October 2022

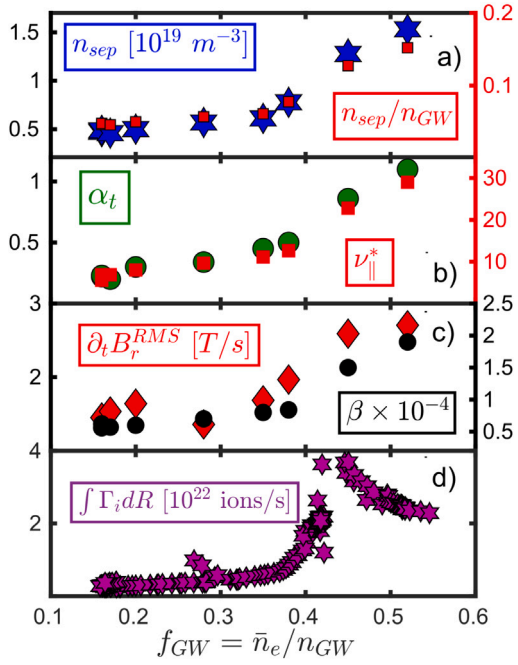

Fig. 1. Greenwald fraction ($f_{GW} = \bar{n}_e/n_{GW}$) dependency on (a) plasma density at the separatrix (n_{sep}) and n_{sep}/n_{GW}, (b) α_t and collisionality ($\nu^*_{\parallel}$), (c) separatrix plasma beta and radial magnetic field fluctuation at the outboard midplane, and (d) integrated ion-flux towards outer divertor.

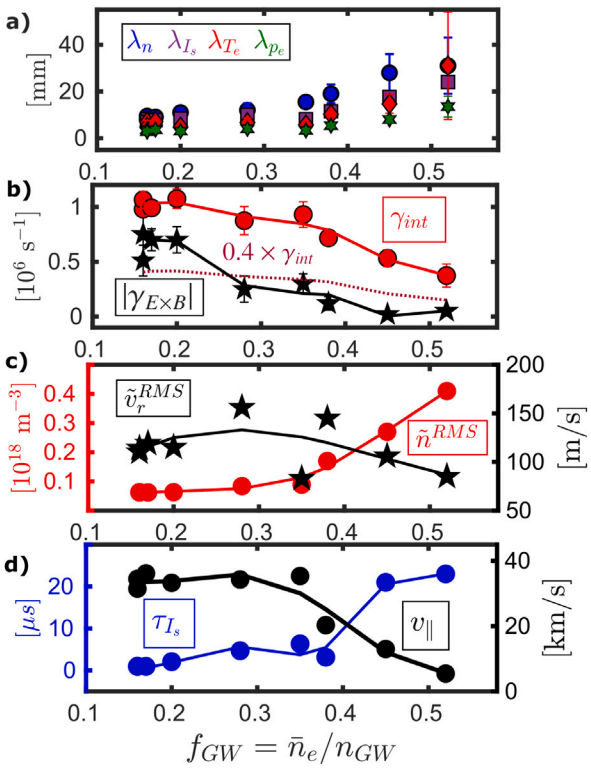

Fig. 2. Near SOL parameters as function of the Greenwald fraction: (a) e-folding lengths of density, ion saturation current, electron temperature, and electron pressure (fitted in the interval $1 \leq \rho_p \leq 1.04$); (b) $E \times B$ shearing rate ($\gamma_{E\times B}$) and linear growth rate of interchange instability (γ_{int}); (c) RMS fluctuation level of radial velocity and plasma density; (d) parallel flow ($v_{\parallel} = M_{\parallel} c_s$) velocity and correlation time of I_s.

Although less efficient, adiabatic coupling, which is an essential mechanism for drift-wave and the diamagnetic stabilization of interchange turbulence, can still be effective there.

Therefore, the near SOL is expected to be a region where turbulence transition might take place with a direct impact on transport and mean profiles, as well as far-SOL filamentary activity.

2. Experimental setup

The experiment was carried out in ASDEX Upgrade (AUG) in lower single null favourable configuration, i.e., with the $B\times\nabla B$ drift direction pointing towards the X-point and the toroidal magnetic field of -2.5 T on-axis. The plasma current was 0.8 MA, with the edge safety factor in the range of 4.5–4.6. The deuterium plasma was externally electron cyclotron resonance heated (ECRH) with 0.3 MW at 140 GHz X-mode, below the L-H transition threshold power.

The edge plasma density was measured by lithium beam spectroscopy, the electron temperature by Thomson scattering, and the radial electric field by Doppler reflectometry. The SOL was monitored with a scanning probe installed on the midplane manipulator. The probe head is composed of three ball-pen probe (BPP) pins poloidally displaced and four Langmuir pins (flush-mounted) arranged in a rectangular array, where opposite pins with respect to the toroidal direction work as a Mach probe [16]. The recessed ball-pen conductor shields parallel electron fluxes along the field lines, making the probe floats near the plasma potential [17]. In addition, by combining Langmuir and ball-pen pins on floating mode, one can measure electron temperature with a high temporal resolution [16].

3. L-mode density scan

A density scan was performed with gas fuelling from the divertor. The central line average density was varied in the range $\bar{n}_e = 1.5 - 5.5 \times 10^{19}$ m^{-3}, corresponding to the Greenwald fraction scan $f_{GW} = \bar{n}_e/n_{GW} = 0.17 - 0.52$, where $n_{GW} = I_p/(\pi a)^2$. Although we did not observe the density limit in these experiments, the maximum achieved density is near the one observed at the L-mode density limit in AUG, $\bar{n}_e/n_{GW} = 0.51 - 0.63$ [11].

Fig. 1(a) shows the density at the separatrix measured with Lithium beam emission spectroscopy (Li-BES) as a function of f_{GW}. n_{sep} increases mildly in the interval $f_{GW} \approx 0.15 - 0.38$ and sharply for larger f_{GW}. The largest n_{sep}/n_{GW} is 0.15. With the rise of the separatrix density, the collisionality also increases (Fig. 1b), with electron temperature dropping from about 55 eV at the lowest density to 45 eV at the highest. The parallel collisionality is defined as $\nu^*_{\parallel} \propto L_c n_e/T_e^2$, where L_c is the parallel connection length, which we approximated to $q\pi R$, where R is the major radius. Likewise, the turbulent parameter $\alpha_t \approx 10^{-2} q \nu^*_{\parallel}$ also increases since the edge safety factor was kept roughly constant in this experiment. The sharp increase of density at the separatrix with a mild reduction of the electron temperature results in the rise of the plasma beta ($\beta = 4\mu_0 T_e n_e/B^2$) there and radial magnetic field fluctuations at the outer midplane (Fig. 1c). This result suggests that turbulence near the density limit becomes more electromagnetic. Finally, the outer divertor starts to detach from $f_{GW} = 0.43$ as the integrated ion flux rolls over and the averaged target electron temperature drops below 5 eV. At roughly same range, density shoulder is formed, as previously observed [18,19].

4. Near SOL evolution

Increasing the plasma density towards the density limit while keeping constant the external heating power leads to the rise of collisionality and plasma beta around the separatrix and the detachment of the outer divertor (Fig. 1). As previously shown in Ref. [20], the increase of α_t is connected to the widening of the near SOL fall-off lengths. Fig. 2(a) confirms these observations. The e-folding lengths of plasma density, ion saturation current, electron temperature, and electron pressure in

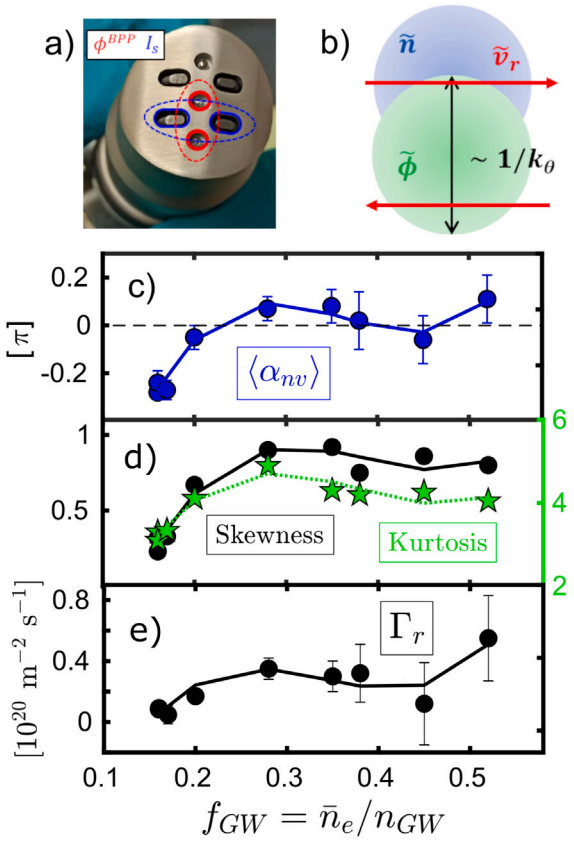

Fig. 3. (a) Ball-pen probe head in a balanced configuration to measure the turbulent particle transport, reducing phase delay errors. (b) The phase shift between density and plasma potential fluctuation results in transport via $E\times B$ drift. Near SOL (c) averaged cross-phase between density and radial velocity fluctuation (α_{nv}), (d) skewness and kurtosis of ion saturation current, and (e) turbulent particle flux (Γ_r) as a function of $f_{GW} = \bar{n}_e/n_{GW}$.

the near SOL ($1 \leq \rho_p \leq 1.04$) rise with f_{GW}. Particularly, a sharp increase occurs from $f_{GW} \approx 0.3$ on.

The gradual cooling of the outer divertor results into the flattening of the plasma potential profile at the outer midplane and the reduction of the radial electric field [21]. Around $f_{GW} \approx 0.35$, the near SOL radial electric field profile (measured with the scanning probe and with Doppler reflectometry) is already entirely flatted. As a result, the $E\times B$ shearing rate, defined as $\gamma^{E\times B} = B^{-1}\partial_r E_r$, weakens. Considering the interchange instability as the dominant one in this region, in Fig. 2(b) we compare its linear growth rate ($\gamma_{int} = c_s/\sqrt{\lambda_p R}$, where $c_s = \sqrt{2T_e/m_i}$) with $|\gamma_{E\times B}|$. In general, $\gamma_{int} > |\gamma_{E\times B}|$. However, as pointed out in [22], for about $|\gamma_{E\times B}| > 0.4\times\gamma_{int}$, interchange instability is already widely stabilized by shear flows. From Fig. 2(b), that seems to be the case for the lowest densities. Besides, with low collisionality and α_t, diamagnetic stabilization would inhibit the growth of the interchange instability [9,10] regardless the background shear flows. Therefore, both effects would stabilize interchange turbulence in the near SOL. This trend reverses at high densities with increasing collisionality and low shear flows.

Density and radial velocity fluctuation ($\tilde{v}_r \approx \tilde{E}_\theta/B_t$, where E_θ is the poloidal electric field and B_t the toroidal magnetic field) are measured with the scanning probe on the midplane manipulator (Fig. 2c). Ion saturation and ball-pen probe potential are used as a proxy for density and plasma potential, respectively. While the velocity does not vary much, density fluctuation (as the root square mean) increases sharply from $f_{GW} \approx 0.35$ on. n^{RMS} increases before the outer divertor detaches, likewise, the autocorrelation time of the ion saturation current fluctuation increases in the same interval (Fig. 2d). Meanwhile, the ion parallel velocity ($v_\parallel = c_s M_\parallel$, where $M_\parallel$ is the parallel Mach number) reduces, especially after detachment. The lower velocity makes the dissipation of density fluctuation less efficient, likely contributing to the further increase of $\tilde{n}^{RMS}$. Near the density limit, the density fluctuation is mostly concentrated at low frequencies, as also observed with thermal helium beam spectroscopy [23].

Radial turbulent transport arises when density perturbation is in phase with the velocity fluctuation pointing radially outward. Therefore, not only the amplitude of the fluctuation impacts the final radial flux, but also the cross-phase, i.e., $\Gamma_r \propto \tilde{n}^{RMS}\tilde{v}_r^{RMS}\cos\alpha_{nv}$, where α_{nv} is the cross-phase between density and radial velocity fluctuation. A favourable cross-phase for transport is obviously when $\alpha_{nv} = 0$, which is the cross-phase for ideal interchange instability [9], e.g., turbulent filaments or blobs are thought to be driven by this type of instability [24]. As discussed in [16], low-frequency fluctuations in the near SOL of AUG typically exhibit interchange character, although the largest coherence might occur at high frequencies in low collisional plasmas where the cross-phase might not be zero. The largest coherence is likely connected with the driven instability. Therefore, we defined an average cross-phase weighted by the cross-coherence between density and radial velocity fluctuation (Fig. 3c). The turbulent particle flux is obtained using the ball-pen probe head in a balanced configuration (Fig. 3a). The density and radial velocity are estimated considering $\tilde{n}_e \propto \tilde{I}_s/\sqrt{\bar{T}_e}$ and $\tilde{v}_r \propto \Delta\tilde{\phi}^{BPP}/d$, where I_s is the ion saturation current, ϕ^{BPP} the ball-pen potential, and d the distance between two BPP pins poloidally displaced. $\langle\alpha_{nv}\rangle$ becomes more interchange-like (i.e. $\langle\alpha_{nv}\rangle \approx 0$) for $f_{GW} = 0.2$. At roughly the same Greenwald fraction, skewness and kurtosis of ion saturation current increase (Fig. 3d), suggesting that density fluctuations become more bursty. Finally, the initial variation of the averaged cross-phase results in an increment of the particle flux, which then saturates for intermediary f_{GW}, increasing again at the highest density (Fig. 3e).

5. Conclusion

We observed a chain of events preceding the density limit. At the lowest densities, $f_{GW} = 0.17$, turbulence had a drift-wave character in the near SOL (just outside the separatrix), while the $E\times B$ shearing rate and parallel flow assume their maximum. At $f_{GW} = 0.20$, a transition to interchange turbulence was observed (based on the averaged cross-phase between density and radial velocity fluctuation), followed by more intermittent density fluctuations. The outer shear layer collapsed at $\bar{n}_e/n_{GW} = 0.35$ as the outer target temperature profiles flatters and the density fluctuation increase. Meanwhile, the parallel flow started to drop, while the plasma beta at the separatrix and radial magnetic field fluctuations at the outer midplane increased. The outer divertor detached at $\bar{n}_e/n_{GW} = 0.45$. In the same range, the SOL parallel Mach number profile became flatter, while the auto-correlation time of density fluctuation increased sharply in the near SOL. Density shoulder formation is observed. At $\bar{n}_e/n_{GW} = 0.5$, cross-field particle transport raised substantially while parallel transport assumed its minimum. At this point, the electron temperature at the separatrix was about 45 eV, while it was approximately 55 eV at the lowest density. In short, the transition leading to the density limit at the near SOL occurs through a chain of events that ultimately involves the progressive increase of cross-field transport. This occurs due to larger density fluctuation amplitude and a transition of the turbulence character from drift-wave to interchange. Furthermore, a reduction of the parallel flow towards the divertor target and weakening of the $E\times B$ shear flow are observed at the highest densities.

CRediT authorship contribution statement

G. Grenfell: Conceptualization, Methodology, Software, Formal analysis, Writing – original draft. **P. Manz:** Conceptualization, Methodology, Writing – review & editing. **G.D. Conway:** Investigation, Data

curation, Validation. **T. Eich:** Validation, Formal analysis, Writing – review & editing. **J. Adamek:** Resources, Methodology. **D. Brida:** Validation, Formal analysis, Writing – review & editing. **M. Komm:** Formal analysis. **T. Nishizawa:** Formal analysis, Writing – review & editing. **M. Griener:** Formal analysis, Investigation. **B. Tal:** Formal analysis, Investigation. **U. Stroth:** Writing – review & editing.

Declaration of competing interest

The authors declare the following financial interests/personal relationships which may be considered as potential competing interests: Gustavo Grenfell reports financial support was provided by Eurofusion.

Data availability

Data will be made available on request.

Acknowledgements

This work has been carried out within the framework of the EUROfusion Consortium, funded by the European Union via the Euratom Research and Training Programme (Grant Agreement No 101052200 — EUROfusion). Views and opinions expressed are however those of the author(s) only and do not necessarily reflect those of the European Union or the European Commission. Neither the European Union nor the European Commission can be held responsible for them.

References

[1] M. Greenwald, J.L. Terry, S.M. Wolfe, S. Ejima, M.G. Bell, S.M. Kaye, G.H. Neilson, A new look at density limits in tokamaks, Nucl. Fusion 28 (12) (1988) 2199.

[2] S. Sudo, Y. Takeiri, H. Zushi, F. Sano, K. Itoh, K. Kondo, A. Iiyoshi, Scalings of energy confinement and density limit in stellarator/heliotron devices, Nucl. Fusion 30 (1) (1990) 11.

[3] D. Fernández-Ruiz, U. Losada, M.A. Ochando, B. Liu, C. Hidalgo, et al., Observation of low frequency electrostatic coherent oscillation in the proximity of the density limit in the TJ-II stellarator, Nucl. Fusion 61 (12) (2021) 126038.

[4] M.E. Puiatti, P. Scarin, G. Spizzo, M. Valisa, R. Paccagnella, I. Predebon, M. Agostini, A. Alfier, A. Canton, S. Cappello, et al., High density limit in reversed field pinches, Phys. Plasmas 16 (1) (2009) 012505.

[5] M. Greenwald, Density limits in toroidal plasmas, Plasma Phys. Controll. Fusion 44 (8) (2002) R27.

[6] B. LaBombard, R.L. Boivin, M. Greenwald, J. Hughes, B. Lipschultz, D. Mossessian, C.S. Pitcher, J.L. Terry, S.J. Zweben, Alcator Group, Particle transport in the scrape-off layer and its relationship to discharge density limit in Alcator C-Mod, Phys. Plasmas 8 (5) (2001) 2107–2117.

[7] O.E. Garcia, J. Horacek, R.A. Pitts, A.H. Nielsen, W. Fundamenski, V. Naulin, J.J Rasmussen, Fluctuations and transport in the TCV scrape-off layer, Nucl. Fusion 47 (7) (2007) 667.

[8] R. Hong, G.R. Tynan, P.H. Diamond, L. Nie, D. Guo, T. Long, R. Ke, Y. Wu, B. Yuan, M. Xu, Edge shear flows and particle transport near the density limit of the HL-2A tokamak, Nucl. Fusion 58 (1) (2017) 016041.

[9] B.D. Scott, Drift wave versus interchange turbulence in tokamak geometry: Linear versus nonlinear mode structure, Phys. Plasmas 12 (6) (2005) 062314.

[10] B.N. Rogers, J.F. Drake, A. Zeiler, Phase space of tokamak edge turbulence, the L- H transition, and the formation of the edge pedestal, Phys. Rev. Lett. 81 (20) (1998) 4396.

[11] T. Eich, P. Manz, The separatrix operational space of ASDEX Upgrade due to interchange-drift-Alfvén turbulence, Nucl. Fusion (2021).

[12] M. Giacomin, A. Pau, P. Ricci, O. Sauter, T. Eich, JET Contributors, et al., First-principles density limit scaling in tokamaks based on edge turbulent transport and implications for ITER, Phys. Rev. Lett. 128 (18) (2022) 185003.

[13] B.N. Rogers, J.F. Drake, Enhancement of turbulence in tokamaks by magnetic fluctuations, Phys. Rev. Lett. 79 (2) (1997) 229.

[14] R.J. Hajjar, P.H. Diamond, M.A. Malkov, Dynamics of zonal shear collapse with hydrodynamic electrons, Phys. Plasmas 25 (6) (2018) 062306.

[15] B. Schmid, P. Manz, M. Ramisch, U. Stroth, Collisional scaling of the energy transfer in drift-wave zonal flow turbulence, Phys. Rev. Lett. 118 (5) (2017) 055001.

[16] G. Grenfell, J. Adamek, M. Komm, D. Brida, G.D. Conway, P. Manz, P. Tolias, T. Eich, A. Herrmann, T. Nishizawa, U. Stroth, the ASDEX Upgrade team, High-heat flux ball-pen probe head in ASDEX-Upgrade, Rev. Sci. Instrum. 93 (2) (2022) 023507.

[17] J. Adámek, J. Stöckel, M. Hron, J. Ryszawy, M. Tichỳ, R. Schrittwieser, C. Ionită, P. Balan, E. Martines, G. Van Oost, A novel approach to direct measurement of the plasma potential, Czech. J. Phys. 54 (3) (2004) C95–C99.

[18] D. Carralero, G. Birkenmeier, H.W. Müller, P. Manz, P. deMarne, S.H. Müller, F. Reimold, U. Stroth, M. Wischmeier, E. Wolfrum and, An experimental investigation of the high density transition of the scrape-off layer transport in ASDEX Upgrade, Nucl. Fusion 54 (12) (2014) 123005.

[19] N. Vianello, D. Carralero, C.K. Tsui, V. Naulin, M. Agostini, I. Cziegler, B. Labit, C. Theiler, E. Wolfrum, D. Aguiam, S. Allan, M. Bernert, J. Boedo, S. Costea, H. De Oliveira, O. Fevrier, J. Galdon-Quiroga, G. Grenfell, A. Hakola, C. Ionita, H. Isliker, A. Karpushov, J. Kovacic, B. Lipschultz, R. Maurizio, K. McClements, F. Militello, A.H. Nielsen, J. Olsen, J.J. Rasmussen, T. Ravensbergen, H. Reimerdes, B. Schneider, R. Schrittwieser, E. Seliunin, M. Spolaore, K. Verhaegh, J. Vicente, N. Walkden, W. Zhang, the ASDEX Upgrade Team, the TCV Team, the EUROfusion MST1 Team, Scrape-off layer transport and filament characteristics in high-density tokamak regimes, Nucl. Fusion 60 (1) (2019) 016001.

[20] T. Eich, P. Manz, R.J. Goldston, Pascale Hennequin, P. David, M. Faitsch, B. Kurzan, B. Sieglin, E. Wolfrum, et al., Turbulence driven widening of the near-SOL power width in ASDEX Upgrade H-Mode discharges, Nucl. Fusion 60 (5) (2020) 056016.

[21] D. Brida, G.D. Conway, T. Eich, G. Grenfell, U. Plank, J. Adamek, M. Komm, EUROfusion MST1 team ASDEX Upgrade team, Physics of the electric field in the scrape-off layer of ASDEX Upgrade L-mode discharges and relation to divertor conditions, PSI (2022).

[22] Y. Zhang, S.I. Krasheninnikov, A.I. Smolyakov, Influence of flow shear on localized Rayleigh–Taylor and resistive drift wave instabilities, Contrib. Plasma Phys. 60 (5–6) (2020) e201900098.

[23] T. Nishizawa, P. Manz, G. Grenfell, M. Griener, D. Wendler, D. Brida, D.M. Kriete, R. Dux, T. Kobayashi, M. Sasaki, et al., Characterizing the flow and turbulence structure near the last closed flux surface in L-mode plasmas of ASDEX Upgrade, Phys. Plasmas 29 (7) (2022) 072304.

[24] S.I. Krasheninnikov, D.A. D'ippolito, J.R. Myra, Recent theoretical progress in understanding coherent structures in edge and SOL turbulence, J. Plasma Phys. 74 (5) (2008) 679–717.